Edge-Guided Multiscale Segmentation of Satellite Multispectral Imagery

Jianyu Chen, Jonathan Li, *Senior Member, IEEE*, Delu Pan, Qiankun Zhu, and Zhihua Mao

***Abstract*—This paper presents a new approach to multiscale segmentation of satellite multispectral imagery using edge information. The Canny edge detector is applied to perform multispectral edge detection. The detected edge features are then utilized in a multiscale segmentation loop, and the merge procedure for adjacent image objects is controlled by a separability criterion that combines edge information with segmentation scale. The significance of the edge is measured by adjacent partitioned regions to perform edge assessment. The present method is based on a half-partition structure, which is composed of three steps: single edge detection, separated pixel grouping, and significant feature calculation. The spectral distance of the half-partitions separated by the edge is calculated, compared, and integrated into the edge information. The results show that the proposed approach works well on satellite multispectral images of a coastal area.**

***Index Terms*—Edge detection, multiscale segmentation, object-based image analysis, scale selection.**

I. Introduction

THE multiscale segmentation method, initially named the fractal net evolution approach (FNEA) [1], [2], which provides a key technique for extraction of image objects, is based on the fact that most image data contain object-based information [3]. One obvious advantage is that objects as minimum classification units help overcome the problem of salt-and-pepper effects resulting from conventional pixel-based classification methods [4], [5]. However, the procedure of segmentation where pixels are linked to the objects necessarily involves scale [6]. The importance of scale has been addressed in applications such as object-based mapping of vegetation parameters with hyperspectral imagery [7]. Landscape is a complex system composed of a large number of heterogeneous components with varying size and shape [8]. A certain scale used in segmentation does not yield a perfect partition of the scene but produces either too many small regions (oversegmentation) or too few large segments (undersegmentation). Thus, a segmentation scheme was designed [9] in which objects were generated at many different scales in order to determine optimal scale parameters.

In some cases, researchers have tried to display the whole scene in one layer. Burnett and Blaschke [5] developed a methodology called as Multi Scale Segmentation/Object Related Modelling (MSS/ORM) to simultaneously derive objects at several levels of segmentation detail. Lang and Langanke [10] showed a one-level representation that might be sufficient and more straightforward. Hay *et al.* [11], [12] developed an object-specific upscaling methodology. Chen *et al.* [13], [14] tried to identify a meaningful image object by calculating its difference distinctive feature in each loop of MSS. The appropriate scale of observation is a function of the type of environment and information that is being sought. Scale selection is still very important and is a hot research topic in object-based image analysis [15]. This paper proposes an edge-guided MSS approach that performs unsupervised scale selection in object-based analysis. The methodology is integrated with edge detection and region extraction adapted to uniform and/or weakly textured remote-sensed imagery.

It is well known that regions and edges are the two key features in visual perception. Approaches based on region and edge features are based on two fundamental observations [16]: discontinuity and similarity. Technically, edge detection methods place emphasis on discontinuity and locate the meaningful intensity discontinuity by using spatial differentiation or edge template operations. However, the edge detection methods suffer from the fact that the edge pixels produced by the edge detectors are discontinuous and seldom characterize a region completely. Therefore, image segmentation is conceptually based on similarity. In order to overcome the difficulties to obtaining satisfying image partitioning results by using only one segmentation method, cooperative approaches [17]–[19] were based on combination and integration of several methods. These techniques [20], [21] have been proposed to generate a coherent and stable image representation in hierarchical or multiscale image segmentation. The additional information obtained from edge or regions [22]–[24] has been used to eliminate the uncertainty [25], [26] of segmentation and object evaluation [27], [28]. These complementary results tried to fulfill the weaknesses of each of the different segmentation methods. The methodology presented here therefore uses integrated edge detection and MSS, and is almost automatic and unsupervised. This integration allows us to exploit the

Manuscript received August 30, 2011; revised December 22, 2011, February 3, 2012, and March 19, 2012; accepted March 24, 2012. Date of publication May 23, 2012; date of current version October 24, 2012. This work was supported in part by the National Natural Science Foundation of China under Grants 40976109 and 40606040, by the Key Projects in the National Science and Technology Pillar Program under Grant 2008BAC42B02, by the R&D Special Fund for Public Welfare Industry (Oceanography) under Grant 201005011-2, and by the China Scholarship Council.

J. Chen, D. Pan, Q. Zhu, and Z. Mao are with the State Key Laboratory of Satellite Ocean Environment Dynamics, Second Institute of Oceanography, State Oceanic Administration, Hangzhou 310012, China (e-mail: chinechen@yahoo.com; pandelu@sio.org.cn; zhuqiankun@sio.org.cn; mao@sio.org.cn).

J. Li is with the Department of Geography and Environmental Management, University of Waterloo, Waterloo, ON N2L 3G1, Canada, and also with the Key Laboratory of Underwater Acoustic Communication and Marine Information Technology, School of Information Science and Engineering, Xiamen University, Xiamen 361005, China (e-mail: junli@uwaterloo.edu).

Digital Object Identifier 10.1109/TGRS.2012.2194502

advantages of each method. The performance of this approach has been experimentally demonstrated on coastal remote sensing applications.

The rest of this paper is organized as follows. The mathematical foundation for developing the edge-guided MSS method, including MSS and multispectral edge detection, is introduced in Section II. The exercisable experiments are presented in Section III. This forms a basis for the newly developed edge-guided MSS method, and the details of the newly proposed edge assessment approach are introduced in the subsequent sections. The experimental results obtained using coastal satellite multispectral images are presented and discussed in Section IV. In addition, some conclusions are drawn in Section V.

II. Transform

The FNEA method is considered to be one of the effective region-based segmentation techniques. Technically, FNEA composes of two fundamental components: the generation of a multiscale representation and information extraction [2], [5]. The threshold used to control the segmentation procedure is a combination of size and homogeneity. Given a definition for image fractal homogeneity, the merging criteria for an adjacent object pair is found by calculating the overall fusion value f. Here, it is changed to F in order to satisfy the additional condition G in our method as follows:

$$F = \begin{cases} f, G \leq \varepsilon \\ \infty, G > \varepsilon \end{cases} \tag{1}$$

where G is the measure of edge information and ε is a user-given edge criteria to complete the judgment of separability. G is calculated from the result of the edge detector and can be determined as the following function:

$$G = g(e \cdot p) \tag{2}$$

where e is the measure of edge strength and p works as a correction parameter with regard to the significance of the regions separated by it. Here, by judging the edge point in the interior of object pair A, the function can be briefly specified as follows:

$$g(e \cdot p) = \sum |e \cdot p|, e \in |\mathrm{A}|. \tag{3}$$

Moreover, f can be still represented as follows:

$$f = w \cdot h_{\mathrm{color}} + (1 - w) \cdot h_{\mathrm{shape}} \tag{4}$$

where h_{color} and h_{shape} are the spectral heterogeneity and shape heterogeneity, respectively, and w is the user-defined weight for spectral (against shape) within the range $0 \leq w \leq 1$ (for more details, see [2] or [29]). The color criterion h_{color} is the weighted mean of all changes in standard deviations for each channel c, as given in

$$h_{\mathrm{color}} = \sum_c w_c \left(n_{\mathrm{Merge}} \cdot \sigma_c^{\mathrm{Merge}} - \left(n_{\mathrm{obj1}} \cdot \sigma_c^{\mathrm{obj1}} + n_{\mathrm{obj2}} \cdot \sigma_c^{\mathrm{obj2}} \right) \right) \tag{5}$$

where σ_c is the standard deviation and n_{obj} is the object size. The shape criterion h_{shape} consists of smoothness and compactness, which can be computed by

$$h_{\mathrm{shape}} = w_{\mathrm{cmpct}} \cdot h_{\mathrm{cmpct}} + (1 - w_{\mathrm{cmpct}}) \cdot h_{\mathrm{smooth}} \tag{6}$$

where w_{cmpct} is the user-defined weight for the compactness criterion with $0 \leq w_{\mathrm{cmpct}} \leq 1$. Again, the change in shape heterogeneity caused by merging is evaluated by calculating the differences between the situation after and before the merge

$$h_{\mathrm{cmpct}} = n_{\mathrm{Merge}} \cdot \frac{l_{\mathrm{Merge}}}{\sqrt{n_{\mathrm{Merge}}}} - \left(n_{\mathrm{obj1}} \cdot \frac{l_{\mathrm{obj1}}}{\sqrt{n_{\mathrm{obj1}}}} + n_{\mathrm{obj2}} \cdot \frac{l_{\mathrm{obj2}}}{\sqrt{n_{\mathrm{obj2}}}} \right) \tag{7}$$

$$h_{\mathrm{smooth}} = n_{\mathrm{Merge}} \cdot \frac{l_{\mathrm{Merge}}}{b_{\mathrm{Merge}}} - \left(n_{\mathrm{obj1}} \cdot \frac{l_{\mathrm{obj1}}}{b_{\mathrm{obj1}}} + n_{\mathrm{obj2}} \cdot \frac{l_{\mathrm{obj2}}}{b_{\mathrm{obj2}}} \right) \tag{8}$$

where n denotes the object size, l is the object perimeter, and b is the perimeter of the bounding box of the object.

Edge strength e is obtained from the edge detector as a measure of local discontinuity. The Canny edge detector [30] is considered as a state-of-the-art edge detector. In addition, its variation [31], which is particularly developed for multispectral remote-sensed imagery, considered the problem of multidimensional imagery in vector space. Let us consider the multispectral image function $\mathbf{C}$ and the direction $\boldsymbol{r}$, which is defined by the angle φ. While an intensity image function would only have one component, a multispectral function $\mathbf{C}(x, y)$ forms a vector of m scalars at each image position as follows:

$$\overrightarrow{C}(x, y) = \begin{pmatrix} C_1(x, y) \\ \dots \\ Cm(x, y) \end{pmatrix} \quad \overrightarrow{r} = \begin{pmatrix} \cos\varphi \\ \sin\varphi \end{pmatrix}. \tag{9}$$

The directional derivative of the vector-valued function $\overrightarrow{C}$ again gives a vector that consists of the directional derivatives of each component of $\overrightarrow{C}$. The first directional derivative of $\overrightarrow{C}$ can be denoted in the following way:

$$\frac{\partial \overrightarrow{C}}{\partial \overrightarrow{r}} = \begin{pmatrix} \frac{\partial C_1}{\partial \overrightarrow{r}} \\ \dots \\ \frac{\partial C_m}{\partial \overrightarrow{r}} \end{pmatrix} = \begin{pmatrix} \nabla C_1 \cdot \overrightarrow{r} \\ \dots \\ \nabla C_1 \cdot \overrightarrow{r} \end{pmatrix} = \begin{pmatrix} C_{1x} & C_{1y} \\ \dots & \dots \\ C_{mx} & C_{my} \end{pmatrix} \cdot \overrightarrow{r} = J \cdot \overrightarrow{r}. \tag{10}$$

The matrix J containing the derivatives of each component of $\overrightarrow{C}$ is called the Jacobian matrix. A gradient-like solution would then be obtained by determining that direction $\boldsymbol{r}$, which corresponds to a maximum value of change. It turns out to be mathematically attractive to define the magnitude of change through the Euclidean length L of the vector $J \cdot \overrightarrow{r}$ as follows:

$$L^2 = \|J \cdot \overrightarrow{r}\|^2 = (J \cdot \overrightarrow{r})^T \cdot (J \cdot \overrightarrow{r}) = \overrightarrow{r}^T \cdot (J^T \cdot J) \cdot \overrightarrow{r}. \tag{11}$$

Thus, by maximizing L^2 as a function of $\vec{r}$, the following coefficients describing the symmetric 2×2 matrix $J^T J$ is

$$J^T \cdot J = \begin{pmatrix} a_{11} & a_{12} \\ a_{21} & a_{22} \end{pmatrix} \quad \text{where} \tag{12}$$

$$a_{11} = C_{1x}^2 + \cdots + C_{mx}^2$$
$$a_{22} = C_{1y}^2 + \cdots + C_{my}^2$$
$$a_{12} = C_{1x}C_{1y} + \cdots + C_{mx}C_{my}$$
$$a_{21} = a_{12}.$$

As it can be seen that the term $\vec{r}^T \cdot (J^T \cdot J)\, \vec{r}$ is equivalent to the Rayleigh quotient of the matrix $J^T J$. Locally estimating the direction and magnitude of the strongest change in a multidimensional image function can be regarded as an eigenvalue problem. As long as the image function $\mathbf{C}$ is defined on two spatial dimensions (x and y), there exist only two eigenvalues λ_1 and λ_2, where $\lambda_{\max} = \max(|\lambda_1|, |\lambda_2|)$ is given by

$$\lambda_{\max} = \frac{1}{2} \cdot \left((a_{11} + a_{22}) + \sqrt{(a_{11} + a_{22})^2 + 4a_{12}^2} \right). \tag{13}$$

The direction of the corresponding eigenvector can be derived from the eigenvector equation and the results in

$$\varphi_{\max} = \arctan\left(\frac{\lambda_{\max} - a_{11}}{a_{12}} \right). \tag{14}$$

Here, the direction angle $\varphi_{\max}$ is used to compute the gradient magnitudes in the x-direction and in the y-direction, which would be utilized in the next Canny edge detection procedure.

Upon specifying values for "high_threshold" and "lower_threshold" in the algorithm, then

If $(\lambda_{\max} \geq$ high_threshold$) e = 1$

Else if $(\lambda_{\max} <$ lower_threshold$) e = 0$

Else $e = (\lambda_{\max} -$ lower_threshold$)/($high_threshold $-$ lower_threshold$)$.

Moreover, the edge strength e is adjusted by the local parameter p. The value of p is calculated by a half-partition structure, which is separated by the edge. Then, the difference of the partitioned regions can be calculated as follows:

$$d = \sqrt{\sum_c (v_{1c} - v_{2c})^2} \tag{15}$$

where d is the spectral distance of two partitions 1 and 2 separated by edge and v is the mean value of partition for each channel c. For each edge, let σ_1 and σ_2 be the standard deviation of two partitions adjacent to the edge, where modification factor of edge strength is assumed to be a parameter p.

If $(d \geq \max(\sigma_1, \sigma_2)) p = 1$

Else if $(d < \min(\sigma_1, \sigma_2)) p = 0.5$

Else $p = 0.75$

The edge strength derived from the edge detector is adjusted by the local parameter p.

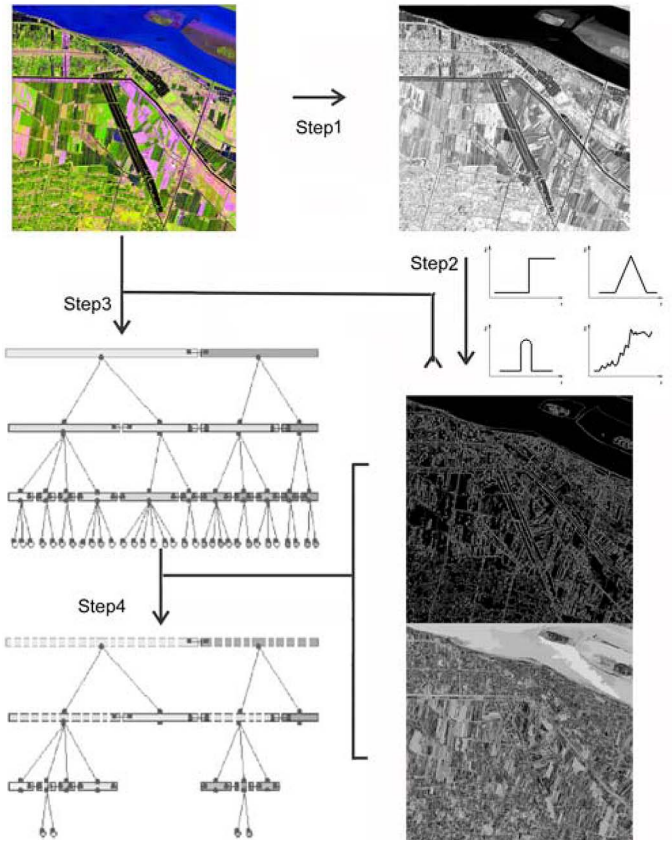

Fig. 1. Depiction of our approach for integrating edge detection and multiscale segmentation. The method mainly includes four steps: 1) application of preprocessing-like dimensionality reduction and noise filters; 2) application of the Canny edge detector to detect edges on the original multispectral image or its processed results; 3) the performance of multiscale segmentation from a minimum scale to a relatively large scale, where the merge of the image objects relies on the edge strength between them; 4) the presentation of the potential meaningful image objects in multiscale analysis.

III. Experiments

The proposed approach (see Fig. 1) consists of four main procedures: 1) preprocessing, including dimensionality reduction and noise filtering; 2) multispectral edge detection; 3) MSS from minimum scale to a relative large scale; and 4) multiscale presentation of the homogenous candidates or potential meaningful image objects. The result of edge detection performs a controlling function in the MSS procedure as a substitute for scale. The edge detector plays an important role in edge-guided MSS. The algorithm used in our experiments follows a detection scheme, which was proposed by John F. Canny. The Canny edge detector works in a multistage process.

The scheme includes the following.

1) Calculating $\lambda_{\max}$ and $\varphi_{\max}$: For each component of imagery, the performance includes: 1) computing the directional derivatives with Gaussian smoothing and 2) calculating a_{11}, a_{22}, a_{12}, and a_{21} using gradient magnitude.
2) Extracting directional magnitude values: Edge magnitude values have to be projected and obtained in the x-direction and the y-direction at each image position based on $\lambda_{\max}$ and $\varphi_{\max}$. This information is used in edge linking.

3) Nonmaximal suppression: The process is applied to identify the local maxima. Only pixels with edge strength larger than their two adjacent pixels in the gradient direction are identified as edge candidates. Nonmaximal suppression results in one-pixel wide edge segments.
4) Edge linking: The hysteresis tracking process is further applied with thresholds in which all candidate edge pixels below the lower threshold are labeled as nonedges, and all pixels above the low threshold that can be connected to any pixels above the high threshold through a chain of edge pixels are labeled as edge pixels. Each edge segment should be labeled for the following parameter p estimation.

The gradient magnitude of a Gaussian smoothed image is not a means to separate two ground objects ideally. It would be adjusted by a local parameter p. Thus, a classification-based approach was proposed to optimize the edge detector for image segmentation in remote sensing applications. This research focused on edge partitioning two spatial adjacent homogeneous objects, which belong to different classes. Based on labeled edge segments obtained in edge detection, a half-partition structure is constructed by a loop consisting of three steps (see Fig. 2): a monotone increasing or decreasing edge identification, a separated pixels selection, and a significant feature calculation. In this way, this paper presents a new algorithm to measure the significance of the edge using the pixels of partitioned regions instead of the pixels in the range of the template of the edge detector token as a filter. The edge detection procedure was improved by estimating the difference of adjacent regions in two steps: the horizontal significance process and the vertical significance process. Each significance process can be described as following pseudocode:

{
Construct line half part by scanning point on each line;
Link line half part into half-partition by edge labeling;
Calculate the amount, mean and deviation on each half-partition;
Compute the spectral distance of half-partitions by each edge segment;
Set the values on each edge point;
Estimate local parameter using the significance of each edge point.
}

In the FNEA method, the objects are regions under a certain scale from image segmentation. They are generated by one or more criteria of homogeneity in one or more dimensions, respectively. When there are more than two neighborhood objects fulfilling the merge condition, a region-growing question arises on how to select the best fitting image fractal pair to merge. This should involve searching the whole scene and performing one merge in each repeated loop. The solution adopted in FNEA is a local mutual best fitting region-growing strategy. Further, the scale controlling the segmentation result is enhanced by satisfying edge condition G. Here, we constrict the merge procedure by the additional condition of the strength of the edge between them.

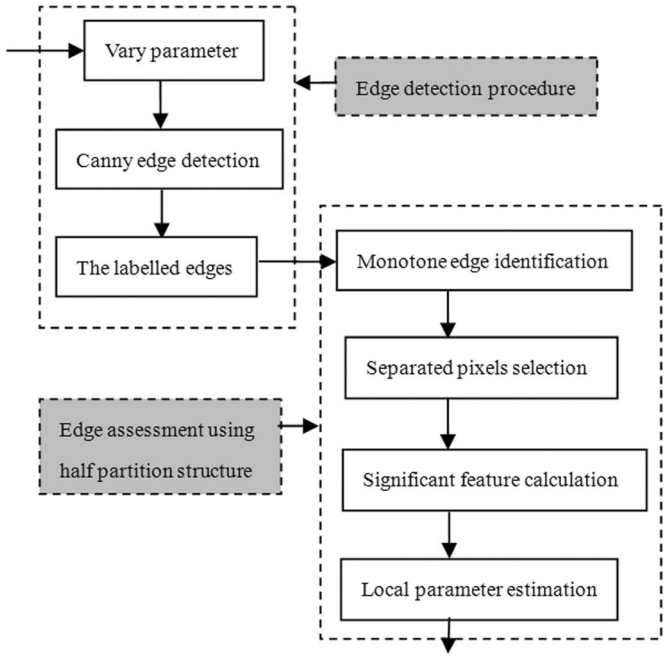

Fig. 2. Edge assessment and local parameter estimation using a half-partition-structure-based approach that consists of three steps: One monotone increasing or decreasing edge identification, separated pixels selection, and significant feature calculation, which follows after a typical edge detector algorithm.

For calculating edge condition G, it should determine the number of edge points on the border between two adjacent regions. Ideally, the description of an image from edge and region primitives must be identical. In practice, the differences are important, and it rarely obtained equivalent descriptions from these two primitives. This duality and complementarity can be expressed in four different ways [32]: 1) the regions are situated in the interior of close contours, and consequently, there are no edge points in the interior of a region; 2) a real edge point must be situated on or at the proximity of a region's boundary; 3) a region's boundary is naturally closed, and an edge boundary should also be closed; 4) an edge cannot be situated in the interior of a region and must be situated on the totality of the common border between two regions. Accordingly, in application, the size of the image object should be larger than the minimum required fulfilling Shannon's sampling pixels, and the distribution of pixel of image object at least fits the 3 × 3-pixel kernel. On the basis of these rules of duality, it can account the edge strength by using once assumed merge: Let ∪ (o) as set of object pair in segmentation procedure. By calculating the interior edge point in the assumed merged object $\mathrm{obj}_{\mathrm{Merge}}$ of pair of obj_1 and its neighbor obj_2, $\cup(\mathrm{o})$ can be divided into$\cup'(\mathrm{o})$ and $\cup g(\mathrm{o})$. For each pair $d \in \cup g(\mathrm{o})$, it meets $g(\mathrm{o}) \leq \varepsilon$, and $F = f$. Then

scale = min_scale;
While size of $(\cup g(\mathrm{o})) > 0$ and scale < max_scale
{
scale+ = Δscale;
MSS performing in $\cup g(\mathrm{o})$;
update $\cup g(\mathrm{o})$;
}

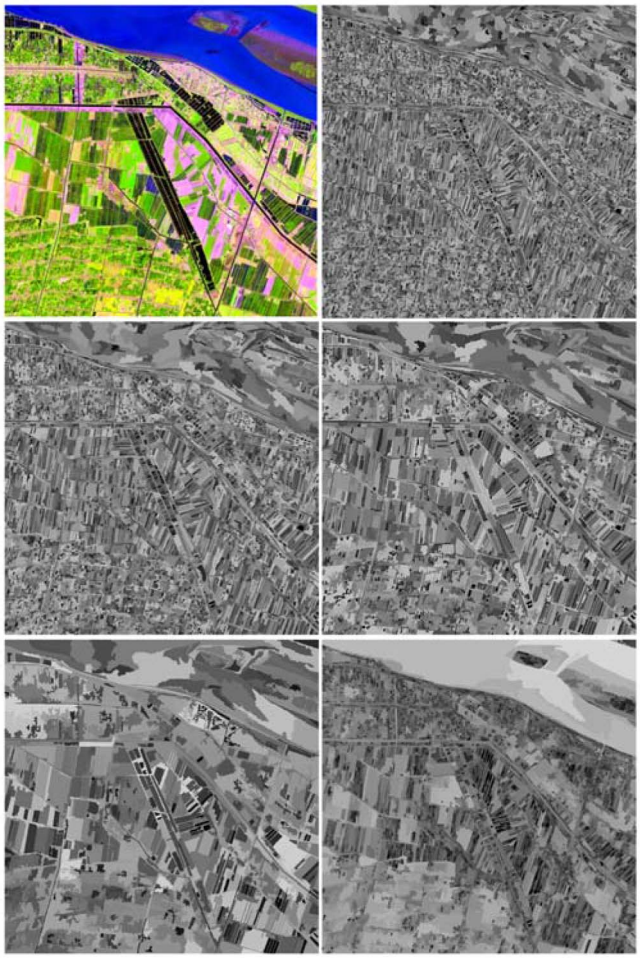

Fig. 3. SPOT5 multispectral image (Red: band4; Green: band1; and Blue: band2) and results at the scales 20, 30, 50 and 100, respectively. The final segmentation is the result of proposed method. The original and segmented images are 1024 × 1024 pixels. The grayscale value of the result indicates the scale of the segmentation (similarly hereinafter).

Fig. 4. Multispectral image of IKONOS, QuickBird2, and Worldview and results by application of proposed method (The original and segmented images are both 800 × 800 pixels.)

Here, the scale is mainly used to determine the sequence of merges in terms of the increase in Δ scale, and it is not a key limitation to prevent merging in the procedure.

IV. Results and Discussion

A. Data set

A 1024 × 1024-pixel subimage of the Satellite pour l'Observation de la Terre (SPOT5) scene acquired on May 7, 2005 is shown in Fig. 3. The area represents a portion of the highly fragmented agro-waterfront landscape. SPOT 5 provides an 8-bit multispectral data in red, green, near-infrared and far-infrared channels at 10-m spatial resolution and an 8-bit panchromatic channel at 5-m resolution. Only the multispectral data have been tested and assessed in image segmentation in this paper. This image is used to test the developed algorithms and to assess the performance of the edge detection process in this paper. IKONOS, QuickBird2, and Worldview satellite multispectral images of a coastal area were also used (see Fig. 4).

B. Edge-Restricted MSS

The result of the proposed approach, as well as results with specified scale, is shown in Fig. 3. Generally, in MSS, a varying scale would be applied to find different types of ground objects with diversity of size and spectral properties. This approach requires a complex designed schema with the aid of masking. In comparison, our approach yielded a single segmentation result, guided by edge information and contained variant scales according to real ground objects. That was, the measure of homogeneity, which given by the segmentation scale, was not a criterion to separate real ground objects basically. The proposed method also has been applied in to three images that were obtained from different sensors and depict typical landscape of coastal area. The scales of regions when they emerged were indicated by the gray value (see Fig. 4). They were also survived and restricted with respect to diverse sizes of ground objects through the whole segmentation procedure, which a relative large scale was set in.

The existing edges prevented regions from being undersegmentation. The size of the image object reflects the real patch of the area by the detected edge. The size of segmented result of agrarian field has been observed larger than the size of residential area. In addition, the scales of image regions show

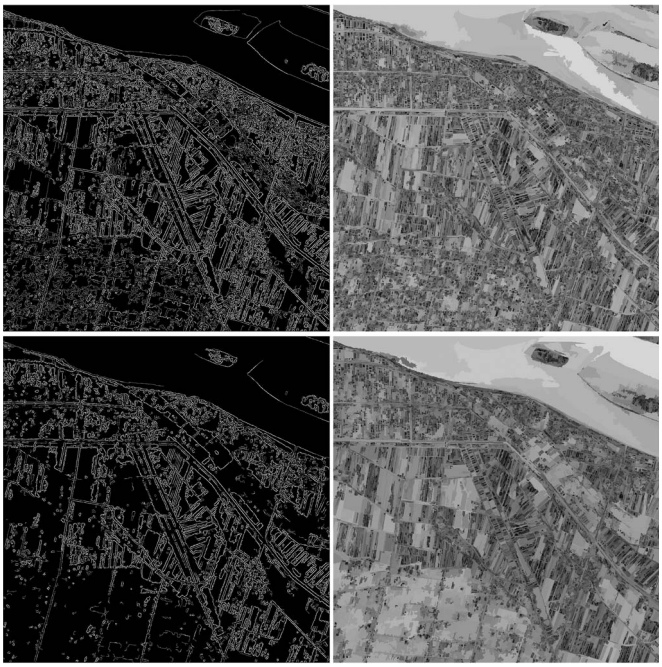

Fig. 5. Detected edge of multispectral image and its constricted multiscale segmentation result. Canny edge detection procedure. Upper (detail): Sigma of the Gaussian filter is 0.4, the ratio of the high threshold is 0.7, and the ratio of the low threshold is 0.3. Below (coarse): Sigma of Gaussian filter is 0.4, the ratio of high threshold is 0.8, and the ratio of low threshold is 0.5.

TABLE I
NUMBER OF PLACES WHERE DETECTED EDGES INTERSECTED IMAGE OBJECTS (OBTAINED FROM NORMAL MSS)

Segment Scale	Objects	Average Size	Intersection by edge
5	1555	307617	837
10	1671	63998	4498
15	952	28432	6843
20	480	16464	6882
25	207	10937	6010
30	99	7819	5043

that there were two types of ponds. The distribution of the scales of our results is more rational compared with the one-scale segmentation result. The detected edges helped to choose the meaningful scales of image objects from the whole multiscale representation. The artificial determination of segmentation scale is avoided. The optimal scale selection in multiscale analysis is reduced to the operation of edge detection. The results (see Fig. 5) of edge-guided MSS of two level details of the detected edge (i.e., detail and coarse) still contained variant image objects. When we overlaid the detected edge with the normal segmented result of the multiscale, there were a large number of intersections between the image objects and detected edges (see Table I). It reveals that the discontinuity and the similarity are not the absolute opposite conception. The segmentation results based on two conceptions are near but not equal.

The scale distribution in this paper shows that there is a double-humped structure of scale of ground objects in this highly fragmented agro-waterfront landscape (see Fig. 6). On

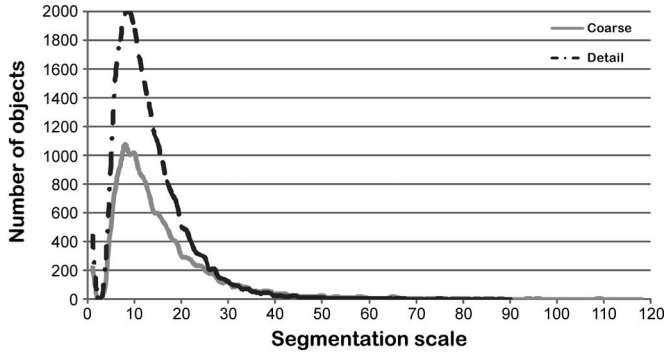

Fig. 6. Statistic distribution of scales of the image objects, and there was a long tail in the coarse case (corresponding to gray images in Fig. 5).

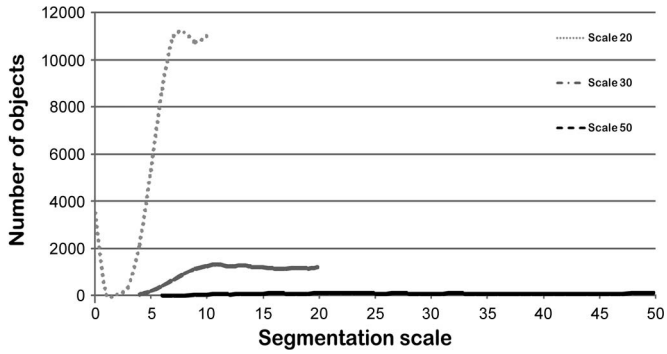

Fig. 7. Statistic distribution of scales of image objects at different segmentation scale in normal multiscale segmentation (corresponding to gray images in Fig. 3).

the contrary, the scale structure of one certain scale segmentation result does not reflect this kind of distribution (see Fig. 7). When the small segmentation scale has been implemented, then the most large ground objects retained over segmentation, and it has not conveyed the advantage of segmentation. The larger scale poses a long tail phenomenon, which means that the smaller scale ground objects keep under segmentation. The result of our method reflects the real structure of scale distribution of ground objects. On that regard, our approach can overcome the limitation that existed in single-scale segmentation.

C. Edge Assessment by Half-Partition Structure

The Canny edges reflect the pixel difference in a short designed range, which is determined by the template of the filter. Nevertheless, this does not really reflect the true spectral difference between these two pixel sets that were separated by edges. The edges by which the separated partitions belonging to different classes are more expected. Considering that, there should be a mechanism to determining interclass and intraclass edges. As most classification methods for remote sensing data are based on the statistical parameter evaluation, with the assumption that samples obey the normal distribution. Based on this hypothesis, this paper assumed that one partition was a sample of one class. At that point, the separated partitions were considered as an approximate estimate of real objects. Each detected edge is coupled with one edge (or boundaries of image) in its left side and restricted a set of pixels as its left partition. In the same way, it restricted its right partition (see Fig. 8). Thus,

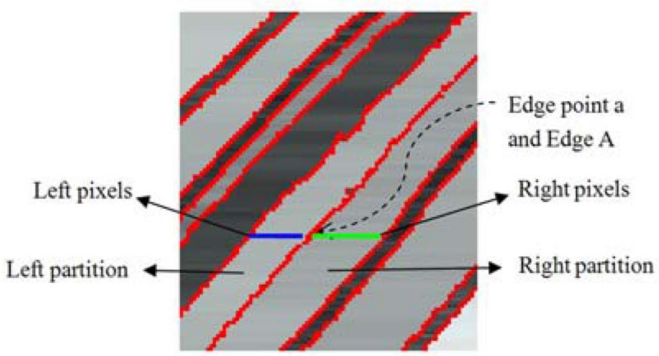

Fig. 8. Edge point and its neighbor edge point can divide a scanning line into several segments. The blue line segment is the left pixels, and the green line segment is the right pixels. In the edge detection procedure, the edge points are linked into the edge, the left pixels are merged into the left partition, and the right pixels are merged into the right partition.

it would face the problem as follows. If we followed edge-point loop clockwise or counterclockwise, the right partition would become the left partition and the left partition would become the right partition at the edge corner. Avoiding this situation, the edges should break in their turn and keep their monotone increasing or decreasing status. Therefore, each scanning line of imagery was divided into several segments, and the segments linked to the same region were regarded as a part of same class.

We dealt with edge information by calculating the mean and the deviation of half-partition limited by two neighbor edges provided by the Canny operator, and then, the pixels in the line segment between each edge couples would divide into two partitions: the left half-partition associated to the left edge and, meanwhile, the right half-partition associated to the right edge. The spectral distance of each partition and its neighborhood was compared mutually, which was used to further determine the significance of the edge that departed them. Through this way, the separability of edges would be enhanced by the spectral distance of the class sample instead of its inherent property of gradient magnitude from using a fixed threshold in the edge detection procedure. According to the image classification in remote sensing, this meant that the significance of meaningful edge could be assessed by calculation of the separability between those two classes essentially. If the mean and the deviation of the both sides of an edge was similar, it meant that the edge would be given a lower significance.

V. Conclusion

In this paper, a new edge-guided MSS has been recommended, trying to perform unsupervised scale selection in object-based analysis. The proposed approach includes four main implementation steps. The merge procedure of two adjacent regions in MSS is constricted by an additional condition of the strength of edge information between them. The performance of the approach was experimentally demonstrated in coastal remote sensing applications. The result of new method reflects the real structure of scale distribution of ground objects in complex areas such as a highly fragmented agro-waterfront landscape. This successfully avoids the shortcoming that exists in one certain scale segmentation result. Edge information is calculated after the application of the Canny edge detector on multispectral imagery extended from monochrome edge detection. As edge performs a controlling role in the segmentation procedure as a substitute for scale, the optimal scale selection in multiscale analysis is reduced to the operation of edge detection.

This paper has also described a new way to measure the significance of the detected edge and to discover the meaningful edges by means of half-partition structure. This is performed and constructed through three algorithms including monotone increasing or decreasing edge identification, separated pixels selection, and significant feature calculation. The half-partitions are regarded as approximate estimates for the sample of class. The spectral distance of separated partition and its neighbors is calculated and compared, which is used to further determine the significance of the edge departed them. Thus, the edges derived from global upper and lower threshold would be adjusted by a local parameter identified by the separability of regions.

Acknowledgment

The authors would like to thank S. Pirasteh and Y. Qin for editorial review, and two anonymous reviewers for their constructive comments.

References

[1] M. Baatz and A. Shäpe, "Object-oriented and multi-scale image analysis in semantic networks," in *Proc. 2nd Int. Symp. Operationalization Remote Sens.*, Enschede, The Netherlands, Aug. 1999, pp. 16–20.

[2] M. Baatz and A. Shäpe, "Multiresolution segmentation, an optimization approach for high quality multi-scale image segmentation," *ISPRS J. Photogramm. Remote Sens.*, vol. 58, no. 3/4, pp. 12–23, Apr. 2000.

[3] T. Blaschke, S. Lang, E. Lorup, J. Strobl, and P. Zei, "Object-oriented image processing in an integrated GIS/remote sensing environment and perspectives for environmental applications," in *Environmental Information for Planning, Politics and the Public*, A. Cremers and K. Greve, Eds. Marburg, Germany: Metropolis Verlag, 2000, pp. 555–570.

[4] Q. Yu, P. Gong, N. Chinton, G. Biging, M. Kelly, and D. Schirokauer, "Object-based detailed vegetation classification with airborne high spatial resolution remote sensing imagery," *Photogramm. Eng. Rem. S.*, vol. 72, no. 7, pp. 799–811, Jul. 2006.

[5] C. Burnett and T. Blaschke, "A multi-scale segmentation/object relationship modeling methodology for landscape analysis," *Ecol. Model.*, vol. 168, no. 3, pp. 233–249, Oct. 2003.

[6] S. Valero, P. Salembier, and J. Chanussot, "New hyperspectral data representation using binary partition tree," in *Proc. IGARSS*, Jul. 2010, pp. 80–83.

[7] E. A. Addink, S. M. Jong, and E. J. Pebesma, "The importance of scale in object-based mapping of vegetation parameters with hyperspectral imagery," *Photogramm. Eng. Remote Sens.*, vol. 73, no. 8, pp. 905–912, Aug. 2007.

[8] J. Wu and J. L. David, "A spatially explicit hierarchical approach to modeling complex ecological systems: Theory and applications," *Ecol. Model.*, vol. 153, no. 1/2, pp. 7–26, Jul. 2002.

[9] Y. Ke, L. J. Quackenbush, and J. Im, "Remote sensing of environment synergistic use of quickbird multispectral imagery and LIDAR data for object-based forest species classification," *Remote Sens. Environ.*, vol. 114, no. 6, pp. 1141–1154, Jun. 2010.

[10] S. Lang and T. Langanke, "Object-based mapping and object-relationship modeling for land use classes and habitats," *Photogramm., Fernerkun., Geoinformation*, vol. 10, no. 1, pp. 5–18, Jan. 2006.

[11] G. J. Hay, D. J. Marceau, P. Dube, and A. Bouchard, "A multiscale framework for landscape analysis: Object-specific analysis and upscaling," *Landscape Ecol.*, vol. 16, no. 6, pp. 471–490, Aug. 2001.

[12] G. J. Hay, G. Castilla, M. A. Wulder, and J. R. Ruiz, "An automated object-based approach for the multiscale image segmentation of forest scenes," *Int. J. Appl. Earth Obsev. Geoinf.*, vol. 7, no. 4, pp. 339–359, Dec. 2005.

[13] J. Chen, D. Pan, and Z. Mao, "Optimum segmentation of simple objects in high- resolution remote sensing imagery in coastal area," *Sci. China (Ser. D)*, vol. 49, no. 11, pp. 1195–1203, Nov. 2006.
[14] J. Chen, D. Pan, and Z. Mao, "Image-object detectable in multiscale analysis on high-resolution remotely sensed imagery," *Int. J. Remote Sens.*, vol. 30, no. 14, pp. 3585–3602, Jul. 2009.
[15] T. Blaschke, "Object based image analysis for remote sensing," *ISPRS J. Photogramm. Remote Sens.*, vol. 65, no. 1, pp. 2–16, Jan. 2010.
[16] D. J. Park, K. M. Nam, and R. H. Park, "Multiresolution edge detection techniques," *Pattern Recognit.*, vol. 28, no. 2, pp. 211–229, Feb. 1995.
[17] C. C. Chu and J. K. Aggarwal, "The integration of image segmentation maps using region and edge information," *IEEE Trans. Pattern Anal. Mach. Intell.*, vol. 15, no. 12, pp. 1241–1252, Dec. 1993.
[18] J. L. Moigne and J. C. Tilton, "Refining image segmentation by integration of edge and region data," *IEEE Trans. Geosci. Remote Sens.*, vol. 33, no. 3, pp. 605–615, May 1995.
[19] M. Mueller, K. Segl, and H. Kaufmann, "Edge- and region-based segmentation technique for the extraction of large man-made objects on high-resolution satellite imagery," *Pattern Recognit.*, vol. 37, no. 8, pp. 1619–1628, Aug. 2004.
[20] P. Arbeláez, M. Maire, C. Fowlkes, and J. Malik, "Contour detection and hierarchical image segmentation," *IEEE Trans. Pattern Anal. Mach. Intell.*, vol. 33, no. 5, pp. 898–916, May 2011.
[21] M. Tabb and N. Ahuja, "Multiscale image segmentation by integrated edge and region detection," *IEEE Trans. Image Process.*, vol. 6, no. 5, pp. 642–655, May 1997.
[22] R. Usamentiaga, D. F. Garcia, and J. Molleda, "Objective comparison of edge detection assessment methods based on genetic optimization," *J. Electron. Imag.*, vol. 18, no. 2, p. 023013, Jun. 2009.
[23] A. Rydberg and G. Borgefors, "Integrated method for boundary delineation of agricultural fields in multispectral satellite images," *IEEE Trans. Geosci. Remote Sens.*, vol. 39, no. 11, pp. 2514–2520, Nov. 2001.
[24] W. Shi, K. Liu, and C. Huang, "A fuzzy-topology-based area object extraction method," *IEEE Trans. Geosci. Remote Sens.*, vol. 48, no. 1, pp. 147–154, Jan. 2010.
[25] A. Lucieer and A. Stein, "Existential uncertainty of spatial objects segmented from satellite sensor imagery," *IEEE Trans. Geosci. Remote Sens.*, vol. 40, no. 11, pp. 2518–2521, Nov. 2002.
[26] X. Zhao, A. Stein, X. Chen, and X. Zhang, "Quantification of extensional uncertainty of segmented image objects by random sets," *IEEE Trans. Geosci. Remote Sens.*, vol. 49, no. 7, pp. 2548–2557, Jul. 2011.
[27] J. S. Cardoso and L. Corte-Real, "Toward a generic evaluation of image segmentation," *IEEE Trans. Image Process.*, vol. 14, no. 11, pp. 1773–1782, Nov. 2005.
[28] R. Unnikrishnan, C. Pantofaru, and M. Hebert, "Toward objective evaluation of image segmentation algorithms," *IEEE Trans. Pattern Anal. Mach. Intell.*, vol. 29, no. 6, pp. 929–944, Jun. 2007.
[29] U. C. Benz, P. Hofmann, G. Willhauck, I. Lingenfelder, and M. Heynen, "Multi-resolution, object-oriented fuzzy analysis of remote sensing data for GIS-ready information," *ISPRS J. Photogramm. Remote Sens.*, vol. 58, no. 3/4, pp. 239–258, Jan. 2004.
[30] J. F. Canny, "A computational approach to edge detection," *IEEE Trans. Pattern Anal. Mach. Intell.*, vol. PAMI-8, no. 6, pp. 679–698, Nov. 1986.
[31] C. Drewniok, "Multi-spectral edge detection. Some experiments on data from Landsat-TM," *Int. J. Remote Sens.*, vol. 15, no. 18, pp. 3743–3765, Dec. 1994.
[32] C. D. Kermad and K. Chehdi, "Automatic image segmentation system through iterative edge–region co-operation," *Image Vis. Comput.*, vol. 20, no. 8, pp. 541–555, Jun. 2002.

Jianyu Chen received the M.Sc. degree in environmental science and the Ph.D. degree in Earth science from Zhejiang University, Hangzhou, China, in 1998 and 2004, respectively.

He is currently a Professor of remote sensing with the State Key Laboratory of Satellite Ocean Environment Dynamics, Second Institute of Oceanography, State Oceanic Administration, Hangzhou. He has been a Postdoctoral Researcher with Shanghai Institute of Technical Physics, Chinese Academy of Sciences. He has also been a Visiting Professor with the Department of Geography and Environmental Management, University of Waterloo, Waterloo, ON, Canada. His research interests include object-based image analysis, remote sensing of coastal environment, and Geographic Information System.

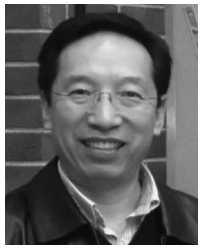

Jonathan Li (M'00–SM'11) received the Ph.D. degree in geomatics engineering from the University of Cape Town, Rondebosch, South Africa, in 2000.

He is currently a Professor with the School of Information Science and Engineering, Xiamen University, Xiamen, China, and a Professor with the Department of Geography and Environmental Management, University of Waterloo, Waterloo, ON, Canada. He is the author of over 170 publications, including more than 60 in refereed journals. His current research interests include Synthetic Aperture Radar (SAR) and Light Detection And Ranging (LiDAR) remote sensing and their innovative applications in environmental monitoring and spatial modeling, primarily focusing on the SAR image analysis for shoreline and oil spill detection, as well as 3-D building extraction from mobile LiDAR point clouds.

Dr. Li is the Chair of International Society of Photogrammetry and Remote Sensing Intercommission Working Group V/I on Land-based Mobile Mapping Systems (2008–2012), Vice Chair of International Cartographic Association Commission on Mapping from Remote Sensor Imagery (2011–2015), and Vice Chair of International Federation of Surveyors Commission IV–Hydrography (2011–2014). He was the recipient of the 2011 Talbert Abrams Award for best paper in photogrammetry and remote sensing from American Society for Photogrammetry and Remote Sensing (ASPRS), the 2008 Environmental Systems Research Institute, Inc. Award for best paper in GIScience from ASPRS, and the 2007 MacDonald, Dettwiler and Associates Award for best paper in photogrammetry and digital mapping from Canadian Institute of Geomatics.

Delu Pan received the B.S. degree in physics from Nanjing University of Science and Technology, Nanjing, China.

He is currently a Senior Scientist (expert of marine remote sensing) with the Second Institute of Oceanography, State Oceanic Administration, Hangzhou, China. He is also an Academician of the Chinese Academy of Engineering and a Professor with Zhejiang University, Hangzhou.

Mr. Pan is the Editor-in-Chief of Acta Oceanologica Sinica (a journal of the Chinese Society of Oceanography) and the Vice President of the Chinese Society of Oceanography. He has been a member of the International Ocean Color Coordinating Group since 2000.

Qiankun Zhu received the B.S. degree in applied mathematics from the Ocean University of China, Qingdao, China.

He is currently a Senior Engineer with the State Key Laboratory of Satellite Ocean Environment Dynamics, Second Institute of Oceanography, State Oceanic Administration, Hangzhou, China. His research interests include remote sensing image analysis and system integration.

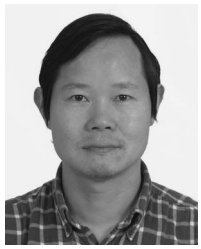

Zhihua Mao received the M.Sc. degree in remote sensing from Zhejiang University, Hangzhou, China, and the Ph.D. degree in physical electronics from Shanghai Institute of Technical Physics, Shanghai, China.

He is currently a Vice Director with the State Key Laboratory of Satellite Ocean Environment Dynamics, Second Institute of Oceanography, State Oceanic Administration, Hangzhou, and a Professor of Earth science with Zhejiang University. His main research interest includes ocean color remote sensing.